

Phonon mediated superconductivity in low carrier-density systems

Maria N. Gastiasoro, Andrey V. Chubukov, and Rafael M. Fernandes
School of Physics and Astronomy, University of Minnesota, Minneapolis, MN 55455, USA.

(Dated: January 23, 2019)

Motivated by the observation of superconductivity in SrTiO₃ and Bi, we analyze phonon-mediated superconductivity in three-dimensional systems at low carrier density, when the chemical potential μ (equal to Fermi energy at $T = 0$) is comparable to or even smaller than the characteristic phonon frequency ω_L . We consider the attractive part of the Bardeen-Pines pairing interaction, in which the frequency-dependent electron-phonon interaction is dressed by the Coulomb potential. This dressing endows the pairing interaction with momentum dependence. We argue that the conventional Migdal-Eliashberg (ME) approximation becomes invalid when $\mu \leq \omega_L$ chiefly because the dominant contribution to pairing comes from electronic states away from the Fermi surface. We obtain the pairing onset temperature, which is equal to T_c in the absence of phase fluctuations, as a function of μ/ω_L . We find both analytically and numerically that T_c increases as the ratio μ/ω_L becomes smaller. In particular, in the dilute regime, $\mu \rightarrow 0$, it holds that $T_c \propto \omega_L \left(\frac{Ry}{\omega_L}\right)^\eta$, where Ry is the Rydberg constant and $\eta \sim 0.2$.

I. INTRODUCTION

Studies of superconductivity in systems with small Fermi surfaces (FSs) attracted a lot of attention over the last decade. The most known and most studied systems of this kind are multi-band quasi-2D Fe-based superconductors with small hole and electron pockets [1]. But superconductivity in 3D systems with small FSs and only one type of carriers also attracted a lot of attention in the past [2–8], and the interest to this issue resurfaced in the last few years [9–23]. The systems of current interest for superconductivity at low electron density include doped SrTiO₃, in which it has been long established that superconductivity is still present at carrier densities as low as $n \sim 10^{18} \text{ cm}^{-3}$ [3, 4, 9], and other materials such as Pb_{1-x}Tl_xTe [5], half-Heusler compounds [10], and single crystal Bi [11]. The observations of superconductivity in these dilute systems motivate the general theoretical investigation of how superconductivity emerges in a system with a small FS and, consequently, small chemical potential μ , counted from the bottom of the band.

The pairing mechanisms in dilute 3D systems are widely debated, and several pairing scenarios have been suggested, particularly for strontium titanate, where superconductivity emerges in the vicinity of a ferroelectric transition [6, 12, 13, 15]. We will not discuss material-specific mechanisms here and instead focus on several general aspects of s-wave pairing due to an exchange of a longitudinal optical phonon with a frequency ω_L .

For systems with sizable electron density, where μ well exceeds ω_L , the analysis of phonon-mediated s-wave pairing is traditionally done using Migdal-Eliashberg (ME) formalism [24–28]. Within this formalism one assumes and then verifies that the pairing involves fermions in the vicinity of the FS, in which case the energy-dependent fermionic density of states can be approximated by its value at the chemical potential, and the dimensionless s-wave pairing component reduces to a constant $\lambda < 0$. One can also verify that the corrections to the pairing

vertex from renormalizations in the particle-hole channel are small in ω_L/μ because in the processes that lead to the vertex renormalization, the fermions are forced to vibrate at phonon frequencies, far away from their own resonance frequencies (this is often termed the adiabatic limit [26, 27, 29]). The ME formalism has been subsequently extended to include the Coulomb repulsion. [26, 27, 30–32] The bare Coulomb repulsion is stronger than the attraction due to phonon exchange, but it extends to frequencies of order μ , while the electron-phonon interaction decays already at frequencies above ω_L . To first approximation, one then has to compare the electron-phonon attraction λ with the effective Coulomb repulsion, renormalized by fermions with energies between μ and ω_L . These renormalizations are logarithmically singular in the particle-particle channel due to the presence of Coulomb logarithm, and they substantially reduce the strength of the Coulomb repulsion and reduce the dimensionless effective Coulomb interaction to a constant u^* . It was argued [32, 33] that $|\lambda| > u^*$, i.e., s-wave phonon-mediated superconductivity survives the Coulomb repulsion. This last point has been verified in more sophisticated calculations [2, 6, 13, 16, 30, 31, 33], where the Coulomb and electron-phonon interactions were treated on equal footing, and the gap equation was solved in the full frequency range of order μ rather than in a narrow range of order ω_L . These calculations have found that the gap function $\Delta(\omega)$ avoids the strong Coulomb repulsion by changing sign as a function of frequency. This is qualitatively similar to how superconductivity emerges in quantum-critical electronic systems, where the pairing emerges from a nominally repulsive interaction mediated by a near-gapless collective boson, e.g, a spin fluctuation [34–40]. The gap function in such systems changes sign between the patches on a given FS, coupled most strongly by a critical boson, or between different Fermi pockets, like cuprate and Fe-based superconductors, respectively. For systems with multiple bands, the sign change between the gaps on different FSs may occur even if superconductivity is predominantly driven

by the electron-phonon interaction. [17, 41–43]

At low electron density, when the characteristic phonon frequency becomes comparable, or even larger than μ , this consideration has to be modified by two reasons. First, the pairing is no longer confined to the FS. Consequently, the equation for the pairing gap becomes a 2D integral equation in frequency and in momentum variation from k_F . Simultaneously, the corrections to the pairing vertex grow and can no longer be rigorously neglected. [7, 8, 14, 22] Second, there is no longer a wide window for downturn renormalization of the Coulomb interaction, hence it is a priori unclear whether the attraction survives when both electron-phonon and Coulomb interaction are treated on equal footing [23]. Recent works proposed alternative sources of pairing in this regime, involving plasmons [6, 13, 16] or the polar coupling to phonons in ionic crystals. [2, 18–21]

In this paper we revisit the electron-phonon pairing problem in a three-dimensional single-band system. Our starting point is the modified Bardeen-Pines (BP) model [44], which treats on equal footing the screened Coulomb repulsion and electron-phonon attraction. The original BP model was introduced for a non-polar crystal, in which case the dressed phonon is an acoustic mode in the low-energy limit. We consider semi-phenomenologically the modified version of the BP model, in which we treat a boson as a gapped mode with a frequency ω_L . The interaction potential in this modified BP model is the sum of a regularly screened Coulomb interaction and an interaction with a gapped dispersionless boson, dressed by the Coulomb potential. The dressing endows the frequency-dependent electron-boson interaction with momentum dependence. Below we will refer to the boson as the longitudinal phonon, but in reality one should view our gapped mode as an excitation hybridized between a longitudinal phonon and a plasmon (see e.g., [13, 16, 45]). In this respect, we note that our semi-phenomenological model is similar to the one rigorously derived for strontium titanate in Ref. [13] for a particular range of model parameters. We do not restrict the parameters (the ratio of ω_L/μ in our case), because our main goal is to understand how superconducting T_c changes between the limits $\omega_L \ll \mu$ and $\omega_L \gg \mu$. We can justify our model in both limits (see Sec. II), but in between our model should be treated as a phenomenological model.

Given the complexity of the problem, here we consider only the attractive part of the interaction and address the issues of vertex corrections and the role of the states away from the FS. We analyze the interplay between the dressed electron-phonon interaction and the Coulomb repulsion in a separate paper. Our main goals here are to find the appropriate computation procedure in the anti-adiabatic limit, when ω_L is larger than μ , and compute the onset temperature of the pairing as a function of the ratio μ/ω_L . We label this temperature T_c with the understanding that it coincides with the actual superconducting T_c only in the absence of phase fluctuations. [46–48]

Within the ME formalism, the pairing is confined to the FS, and T_c in the dilute limit vanishes because λ is proportional to the density of states at the Fermi level, and the latter scales as $\sqrt{\mu}$. We show that the actual result is different because at low carrier densities the pairing comes predominantly from electronic states far away from the FS. In essence, solving for the onset temperature of the pairing at vanishing μ is analogous to solving for a bound state of two fermions in a vacuum. In a 3D system a bound state forms when the attraction exceeds some threshold value. For a bare interaction between electrons and an optical phonon, T_c would vanish at weak enough electron-phonon coupling. However, in the BP model, the electron-phonon interaction is dressed by a Coulomb potential, which becomes progressively less screened as μ decreases. Consequently, the effective electron-phonon coupling gets strongly enhanced and we show that it well exceeds the threshold value. As a result, T_c is non-zero even when $\mu = 0$ and actually exceeds ω_L in this limit. We found analytically and confirmed numerically that in the dilute limit T_c has a polynomial dependence on the phonon frequency ω_L , $T_c \propto \omega_L \left(\frac{Ry}{\omega_L}\right)^\eta$, where Ry is the Rydberg constant and $\eta \sim 0.2$.

Phonon-mediated superconductivity in a system with small Fermi surface has been recently considered in Refs. [49, 50]. In their case the momentum-dependence of the interaction comes primarily from the momentum dependence of the bare electron-phonon coupling, which strongly favors $q = 0$ scattering. The authors of [49, 50] also found that the states away from the Fermi level contribute significantly to the pairing instability. The distinction between our work and Refs. [49, 50] is that they computed T_c numerically, while we obtain the analytical formula for T_c at low fermion density.

The paper is organized as follows. In the next section we introduce the BP model and obtain the equations for the fermionic self-energy and the s-wave component of the pairing vertex. In Sec. III we first solve for T_c within the ME approximation and then investigate the validity of the ME formalism first in the regime $\mu \sim \omega_L$ and then in the dilute limit $\mu \ll \omega_L$. We present the results of the full self-consistent analysis of T_c as a function of μ/ω_L and show that T_c not only remains finite when $\mu = 0$, but actually exceeds ω_L . We summarize our results in Sec. IV.

II. THE MODEL

We consider an isotropic electron gas in 3 dimensions with dispersion $\xi(\mathbf{k}) = \mathbf{k}^2/2m - \mu$. The electrons interact directly via the Coulomb repulsion and indirectly via the exchange of phonons. In the most general case of a polar crystal, there are two optical phonon frequencies, the longitudinal one ω_L and the transverse one ω_T . They are related via the ionic plasma frequency ω_p , as $\omega_L^2 = \omega_T^2 + \omega_p^2$. The RPA expression for the total inter-

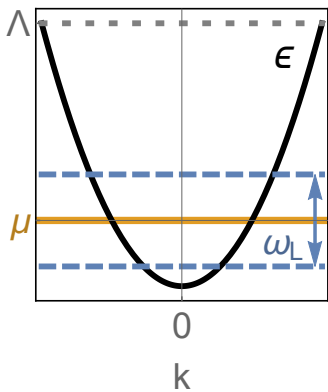


FIG. 1. *The energy scales.* Black line – the parabolic electronic dispersion $\epsilon = k^2/2m$; orange line – the chemical potential μ ; gray dashed line – the bandwidth Λ ; blue dashed lines – the characteristic frequency of the optical phonon ω_L .

action, which includes both the Coulomb and electron-phonon contributions, is given in [13, 45] and is a function of transferred momentum q and transferred frequency Ω . Along the Matsubara axis ($\Omega_n = 2\pi nT$) it is expressed as

$$V_n(\mathbf{q}) = \frac{W_0(\mathbf{q})}{\epsilon_\infty \frac{\Omega_n^2 + \omega_T^2}{\Omega_n^2 + \omega_L^2} - \Pi(\mathbf{q}, \Omega_n) W_0(\mathbf{q})} \quad (1)$$

Here $W_0(\mathbf{q}) = 4\pi e^2/q^2$ is the bare Coulomb repulsion, $\Pi(\mathbf{q}, \Omega_n)$ is the Lindhard function, and ϵ_∞ is the value of the dielectric constant in the large-frequency limit. The ϵ_∞ is related to the zero-frequency value ϵ_0 by $\epsilon_\infty = \epsilon_0 - \omega_p^2/\omega_T^2$ (or, equivalently, $\omega_p^2 = (\epsilon_0 - \epsilon_\infty)\omega_T^2$).

This expression comprises two well-understood regimes. In the case of an insulating ionic crystal, Π can be set to zero, and the effective electron-electron interaction is the Coulomb interaction screened by the polar optical phonons:

$$V_n^{\text{polar}}(\mathbf{q}) = \frac{4\pi e^2}{\epsilon_\infty q^2} \left[1 - \frac{\omega_L^2 - \omega_T^2}{\Omega_n^2 + \omega_L^2} \right] \quad (2)$$

Conversely, in a non-polar crystal, we can set $\omega_T = 0$ and $\epsilon_\infty = 1$ to obtain the BP expression for the dynamical interaction, which vanishes in the static limit. At $\Omega_n \ll v_F q$, $\Pi(\mathbf{q}, \Omega_n)$ can be approximated by its static form, and the BP potential becomes

$$V_n^{BP}(\mathbf{q}) = \frac{4\pi e^2}{q^2 \epsilon(q)} \left[1 - \frac{\omega_q^2}{\Omega_n^2 + \omega_q^2} \right], \quad (3)$$

We set $q \ll k_F$ and used that at small q , $\Pi W_0 \approx 1 - \epsilon(q)$, where $\epsilon(q) = 1 + \frac{\kappa^2}{q^2}$ and $\kappa^2 = 4\pi e^2 N(\mu)$ is the Thomas-Fermi screening momentum expressed via the density of states $N(\mu)$. The frequency ω_q in this approximation is the longitudinal phonon frequency ω_L , renormalized by the electronic polarization: $\omega_q^2 = \omega_L^2/\epsilon(q) = \omega_L^2 q^2/(q^2 +$

κ^2). It becomes an acoustic phonon in the long wavelength limit. Note that ω_L in the BP model is the same as the ionic plasma frequency ω_p , because $\omega_T = 0$.

The authors of [13] considered a polar crystal with a finite density of conduction electrons and obtained the effective $V_n(q)$ by integrating out the phonon degrees of freedom. For parameters relevant to SrTiO₃ they obtained the effective interaction similar to Eq. 3, but with ϵ_0 instead of $\epsilon(q)$ and with a q -independent renormalized electronic plasma frequency instead of ω_q . Because our interest is more general than polar SrTiO₃, we focus instead on the BP limit, Eq. (3). This will allow us to interpolate between the limits $\mu \gg \omega_L$, as appropriate for standard superconductors and $\mu \ll \omega_L$, as appropriate for dilute superconductors.

Importantly, in the remainder of the paper, we will neglect the renormalization of the optical mode ω_L and continue to use the bare frequency ω_L instead of ω_q . The reasoning for this approximation is the following. In the limit of $\mu \gg \omega_L$, the relevant electronic processes are those around the Fermi level, and the renormalization of ω_L by $\epsilon(q)$ can be neglected within the leading logarithmic approximation (see Appendix A). In the opposite limit of very dilute systems $\mu \ll \omega_L$, the screening is negligible and $\epsilon(q) \approx 1$. In between the two limits, the difference between ω_L and ω_q is not negligible, but does not affect the trend of T_c variation with μ/ω_L .

The effective electron-electron interaction $V_n^{BP}(\mathbf{q})$ consists of an instantaneous repulsive screened Coulomb term and a retarded attractive electron-phonon term. Given the complexity of this interaction, in this work we focus on the attractive part of the effective interaction:

$$V_n^{\text{e-ph}}(q) = -\frac{4\pi e^2}{q^2 + \kappa^2} \left[\frac{\omega_L^2}{\Omega_n^2 + \omega_L^2} \right]. \quad (4)$$

We will use the Nambu-Gor'kov formalism in which the pairing vertex is the $\hat{\tau}_1$ piece of the matrix electronic self-energy $\hat{\Sigma}_n(\mathbf{k})$ ($\hat{\tau}_i$ are Pauli matrices). The matrix Dyson equation, relating the Green's function $\hat{\mathcal{G}}_n^{-1}(\mathbf{k})$ to $\hat{\Sigma}_n(\mathbf{k})$, is given by

$$\hat{\mathcal{G}}_n^{-1}(\mathbf{k}) = i\nu_n \hat{\tau}_0 - \xi(\mathbf{k}) \hat{\tau}_3 - \hat{\Sigma}_n(\mathbf{k}) \quad (5)$$

where $\omega_n = (2n + 1)\pi T$ are fermionic Matsubara frequencies. We compute the fermionic self-energy $\hat{\Sigma}_n(\mathbf{k})$ self-consistently by expressing it as a convolution of the interaction $V_{n-n'}^{\text{e-ph}}(|\mathbf{k} - \mathbf{k}'|)$ and the full fermionic propagator $\hat{\mathcal{G}}_{n'}(\mathbf{k}')$:

$$\begin{aligned} \hat{\Sigma}_n(\mathbf{k}) &= -T \sum_{\mathbf{k}', n'} V_{n-n'}^{\text{e-ph}}(|\mathbf{k} - \mathbf{k}'|) \hat{\tau}_3 \hat{\mathcal{G}}_{n'}(\mathbf{k}') \hat{\tau}_3 \\ &= i\omega_n [1 - Z_n(\mathbf{k})] \hat{\tau}_0 + \chi_n(\mathbf{k}) \hat{\tau}_3 + \phi_n(\mathbf{k}) \hat{\tau}_1 \end{aligned} \quad (6)$$

In (6) the self-energy is decomposed into the two 'normal' components, the mass renormalization function $Z_n(\mathbf{k})$

and energy shift $\chi_n(\mathbf{k})$, and the 'anomalous' component (the pairing vertex) $\phi_n(\mathbf{k})$ (Ref. 31). Imposing self-

consistency in Eqs. (5)-(6) we obtain a set of coupled equations for the functions $Z_n(\mathbf{k})$, $\chi_n(\mathbf{k})$ and $\phi_n(\mathbf{k})$,

$$Z_n(\mathbf{k}) - 1 = -T \frac{1}{\omega_n} \sum_{n'} \int \frac{d^3 \mathbf{k}'}{(2\pi)^3} V_{n-n'}^{\text{e-ph}}(|\mathbf{k} - \mathbf{k}'|) \frac{\omega_{n'} Z_{n'}(\mathbf{k}')}{[\omega_{n'} Z_{n'}(\mathbf{k}')]^2 + [\xi(\mathbf{k}') + \chi_{n'}(\mathbf{k}')]^2} \quad (7)$$

$$\chi_n(\mathbf{k}) = T \sum_{n'} \int \frac{d^3 \mathbf{k}'}{(2\pi)^3} V_{n-n'}^{\text{e-ph}}(|\mathbf{k} - \mathbf{k}'|) \frac{\xi(\mathbf{k}') + \chi_{n'}(\mathbf{k}')}{[\omega_{n'} Z_{n'}(\mathbf{k}')]^2 + [\xi(\mathbf{k}') + \chi_{n'}(\mathbf{k}')]^2} \quad (8)$$

$$\phi_n(\mathbf{k}) = -T \sum_{n'} \int \frac{d^3 \mathbf{k}'}{(2\pi)^3} V_{n-n'}^{\text{e-ph}}(|\mathbf{k} - \mathbf{k}'|) \frac{\phi_{n'}(\mathbf{k}')}{[\omega_{n'} Z_{n'}(\mathbf{k}')]^2 + [\xi(\mathbf{k}') + \chi_{n'}(\mathbf{k}')]^2}. \quad (9)$$

We linearized the equations with respect to the pairing vertex $\phi_n(\mathbf{k})$ to compute the superconducting temperature. The computations are simplified by the fact that the interaction $V_{n-n'}^{\text{e-ph}}(|\mathbf{k} - \mathbf{k}'|)$ is factorized between momentum and frequency dependencies: $V_{n-n'}^{\text{e-ph}}(|\mathbf{k} - \mathbf{k}'|) = u_{n-n'} \mathcal{V}(|\mathbf{k} - \mathbf{k}'|)$, where

$$u_{n-n'} = \frac{\omega_L^2}{\omega_L^2 + |\omega_n - \omega_{n'}|^2}; \quad (10)$$

$$\mathcal{V}(|\mathbf{k} - \mathbf{k}'|) = -\frac{4\pi e_0^2}{|\mathbf{k} - \mathbf{k}'|^2 + \kappa^2}.$$

For a rotationally-isotropic fermionic dispersion, which we consider here, $\mathcal{V}(|\mathbf{k} - \mathbf{k}'|)$ and the pairing vertex $\phi_n(\mathbf{k})$ can be expanded in partial components for different angular momentum l . The fermionic $Z_n(\mathbf{k})$ and the energy shift $\chi_n(\mathbf{k})$ depend on the magnitude of momentum $|\mathbf{k}|$, but not on its direction, and are expressed

in terms of the s -wave component of the interaction $v(k, k') = \frac{1}{2\pi} \int_{-1}^1 dx \mathcal{V}(\sqrt{k^2 + k'^2 - 2kk'x})$. The equations for different partial harmonics of $\phi_n(\mathbf{k})$ decouple, and we focus on the s -wave solution for the pairing vertex $\phi_n^s(\mathbf{k}) \equiv \phi_n(k)$. The momentum component of the pairing interaction for $\phi_n(k)$ is the same for $Z_n(k)$ and $\chi_n(k)$.

Below we rescale all variables by the characteristic phonon frequency, i.e., introduce the rescaled temperature $\bar{T} = \frac{T}{\omega_L}$, rescaled Matsubara frequency $\bar{\omega}_n = \frac{\omega_n}{\omega_L}$, rescaled energy $\bar{\epsilon} = \frac{k^2/2m}{\omega_L}$, rescaled $\bar{\kappa}^2 = \frac{\kappa^2/2m}{\omega_L}$, rescaled chemical potential $\bar{\mu} = \frac{\mu}{\omega_L}$, rescaled bandwidth $\bar{\Lambda} = \frac{\Lambda}{\omega_L}$ (the cutoff in momentum space), and $\bar{\rho} = \frac{\text{Ry}}{\omega_L}$, the rescaled variable of the Rydberg energy $\text{Ry} = \frac{me^4}{2} = 13.6$ eV. In these notations, the set of coupled equations for $Z_n(\bar{\epsilon})$, $\bar{\chi}_n(\bar{\epsilon})$, and s -wave pairing potential $\phi_n(\bar{\epsilon})$ are

$$Z_n(\bar{\epsilon}) - 1 = \bar{T} \frac{1}{\bar{\omega}_n} \sum_{n'} u_{n-n'} \int_0^{\bar{\Lambda}} d\bar{\epsilon}' N(\bar{\epsilon}') v(\bar{\epsilon}, \bar{\epsilon}') \frac{\bar{\omega}_{n'} Z_{n'}(\bar{\epsilon}')}{[\bar{\omega}_{n'} Z_{n'}(\bar{\epsilon}')]^2 + [\bar{\epsilon}' - \bar{\mu} + \bar{\chi}_{n'}(\bar{\epsilon}')]^2} \quad (11)$$

$$\bar{\chi}_n(\bar{\epsilon}) = -\bar{T} \sum_{n'} u_{n-n'} \int_0^{\bar{\Lambda}} d\bar{\epsilon}' N(\bar{\epsilon}') v(\bar{\epsilon}, \bar{\epsilon}') \frac{\bar{\epsilon}' - \bar{\mu} + \bar{\chi}_{n'}(\bar{\epsilon}')}{[\bar{\omega}_{n'} Z_{n'}(\bar{\epsilon}')]^2 + [\bar{\epsilon}' - \bar{\mu} + \bar{\chi}_{n'}(\bar{\epsilon}')]^2} \quad (12)$$

$$\phi_n(\bar{\epsilon}) = \bar{T} \sum_{n'} u_{n-n'} \int_0^{\bar{\Lambda}} d\bar{\epsilon}' N(\bar{\epsilon}') v(\bar{\epsilon}, \bar{\epsilon}') \frac{\phi_{n'}(\bar{\epsilon}')}{[\bar{\omega}_{n'} Z_{n'}(\bar{\epsilon}')]^2 + [\bar{\epsilon}' - \bar{\mu} + \bar{\chi}_{n'}(\bar{\epsilon}')]^2}, \quad (13)$$

where $N(\bar{\epsilon}) = \sqrt{\bar{\epsilon}}$ is the density of states and the s -wave component of the interaction is

$$v(\bar{\epsilon}, \bar{\epsilon}') = \frac{\sqrt{\bar{\rho}}}{2\pi\sqrt{\bar{\epsilon}\bar{\epsilon}'}} \log \left[\frac{(\sqrt{\bar{\epsilon}} + \sqrt{\bar{\epsilon}'})^2 + \bar{\kappa}^2}{(\sqrt{\bar{\epsilon}} - \sqrt{\bar{\epsilon}'})^2 + \bar{\kappa}^2} \right]. \quad (14)$$

For further details of the derivation of these equations see Appendix B. We emphasize that the chemical potential $\bar{\mu}$ in Eqs. (11)-(13) is defined at \bar{T}_c rather than

at $T = 0$, where it is equal to the (rescaled) Fermi energy. The value of $\bar{\mu}$ at \bar{T}_c is smaller than at $T = 0$. We will obtain \bar{T}_c as a function of $\bar{\mu}$ at \bar{T}_c and set minimal $\bar{\mu} = 0$. The Fermi energy for such minimal $\bar{\mu}$ is still finite. Throughout this work we will set $\omega_L = 100$ meV and $\bar{\Lambda} = 100$, unless otherwise stated. The numerical solution of the integral equations were computed by using the Nyström method with a N-point Gauss-Legendre

rule ($100 < N < 200$).

In the following section we revisit the computation of the electronic self-energy within the Migdal-Eliashberg (ME) approximation. In this approximation, the temperature variation of $\bar{\mu}$ is neglected, and the integration over $\bar{\epsilon}'$ is confined to the FS, in which case $N(\bar{\epsilon}')v(\bar{\epsilon}, \bar{\epsilon}')$ can be approximated by its value at the Fermi energy. Then the electronic self-energy is independent of $\bar{\epsilon}$, i.e. $\hat{\Sigma}_n(\bar{\epsilon}) = \hat{\Sigma}_n$, and the energy shift $\bar{\chi}_n(\bar{\epsilon})$ reduces to a constant and can be absorbed into the chemical potential. This eliminates the variable $\bar{\epsilon}$ from the Eliashberg equations and reduces them to integral equations only in Matsubara frequency. The ME approximation is fully justified when the characteristic frequency ω_L is small compared to the Fermi energy of the electrons, i.e., $\bar{\mu} \gg 1$, as corrections are small in $1/\bar{\mu}$. [Corrections to the fermion-boson vertex, which we did not include into Eqs. (7)-(9), are also small in $1/\bar{\mu}$.] We investigate the validity of ME approximation as $\bar{\mu}$ gets smaller. We show that the key new effect at small $\bar{\mu}$ is that one cannot restrict the integration over $\bar{\epsilon}'$ to the FS and approximate $N(\bar{\epsilon}')v(\bar{\epsilon}, \bar{\epsilon}')$ by its value at the Fermi energy. Instead one should solve Eqs. (7)-(9) as integral equations in both Matsubara frequency ω_n and the energy variable ϵ . Other deviations from ME approximation are at most $O(1)$ and are not fundamentally relevant.

III. THE RESULTS

A. Standard ME approximations

To be more precise, the ME theory is based on two approximations, both justified by the smallness of the characteristic frequency ω_L compared to the Fermi energy of the electrons:

1. The energy dependent $N(\bar{\epsilon}')v(\bar{\epsilon}, \bar{\epsilon}')$ is replaced by a constant $N(\bar{\mu})v(\bar{\mu}, \bar{\mu})$ as relevant scattering is assumed to be restricted to frequencies of order ω_L . In Fig. 2(a) we plot $N(\bar{\epsilon}')v(\bar{\epsilon}, \bar{\epsilon}')$ in a $\pm 5\omega_L$ energy window around the chemical potential for $\bar{\mu} = 10$. We see that $N(\bar{\epsilon}')v(\bar{\epsilon}, \bar{\epsilon}')$ is indeed close to $N(\bar{\mu})v(\bar{\mu}, \bar{\mu})$.
2. The integration over $\bar{\epsilon}' - \bar{\mu}$ in the r.h.s. of Eqs. (11), (12), and (13) is extended to infinite limits, from $-\infty$ to $+\infty$. Within this approximation, $\bar{\chi}_n = 0$, and the r.h.s. of the equation for the quasiparticle residue Z_n becomes independent of $Z_{n'}$, i.e., it could be computed using free-fermion propagators.

Within these two approximations the set of Eliashberg equations for \bar{T}_c reduces to two integral equations for the

mass renormalization Z_n and the pairing vertex ϕ_n :

$$Z_n = 1 + \lambda \frac{\pi \bar{T}}{\bar{\omega}_n} \sum_{n'} \frac{\text{sgn}(\bar{\omega}_{n'})}{1 + |\bar{\omega}_{n'} - \bar{\omega}_n|^2} \quad (15)$$

$$\phi_n = \lambda \pi \bar{T} \sum_{n'} \frac{1}{1 + |\bar{\omega}_{n'} - \bar{\omega}_n|^2} \frac{\phi_{n'}}{|\bar{\omega}_{n'}| Z_{n'}}. \quad (16)$$

Here

$$\lambda \equiv N(\bar{\mu})v(\bar{\mu}, \bar{\mu}) = \frac{1}{2\pi} \sqrt{\frac{\text{Ry}}{\mu}} \log \left[1 + \pi \sqrt{\frac{\mu}{\text{Ry}}} \right], \quad (17)$$

is a dimensionless coupling constant. It increases monotonically when the chemical potential is reduced and in the limit $\bar{\mu} \rightarrow 0$ reaches $\lambda(\bar{\mu} \rightarrow 0) = 0.5$. This increase is a consequence of the reduced Thomas-Fermi screening length of the electron gas at smaller electronic densities. We show λ as a function of $\bar{\mu}$ in Fig. 3(a) (red line).

The set of the two equations (15) and (16) can be reduced to one integral equation for \bar{T}_c by introducing the superconducting order parameter $\Delta_n \equiv \frac{\phi_n}{Z_n}$, expressing ϕ_n via Δ_n , and substituting the explicit form of Z_n from Eq. (15). This yields a 1D integral equation for Δ_n :

$$\Delta_n = \lambda \pi \bar{T} \sum_{n'} \frac{1}{1 + |\bar{\omega}_{n'} - \bar{\omega}_n|^2} \left(\frac{\Delta_{n'}}{|\bar{\omega}_{n'}|} - \frac{\Delta_n}{|\bar{\omega}_n|} \text{sgn} \omega_{n'} \right). \quad (18)$$

This equation has been extensively studied in the literature. The \bar{T}_c^{ME} , obtained by numerically solving Eq. (18), is shown in Fig. 3(b) (red circles) as a function of the chemical potential $\bar{\mu}$, which enters the gap equation through λ . As the chemical potential is reduced, the critical temperature steadily increases. This growth is expected because the coupling constant λ increases with decreasing μ (see Fig. 3(a)).

At small λ , the quasiparticle residue Z_n does not depend on n to first order in λ : $Z_n = 1 + \lambda + \mathcal{O}(\lambda^2)$. If we use this Z_n , we simplify the equation for \bar{T}_c even further, to

$$\phi_n = \lambda^* \pi \bar{T} \sum_{n'} \frac{1}{1 + |\bar{\omega}_{n'} - \bar{\omega}_n|^2} \frac{1}{|\bar{\omega}_{n'}|} \phi_{n'} \quad (19)$$

where $\lambda^* = \frac{\lambda}{1+\lambda}$. This equation can be solved analytically, again by expanding in the coupling [51–54] and yields

$$\bar{T}_c^{\text{An.sc-ME}} = \frac{1.13}{\sqrt{e}} e^{-\frac{1}{\lambda^*}} = 0.7 e^{-\frac{1+\lambda}{\lambda}} \quad (20)$$

We plot this $\bar{T}_c^{\text{An.sc-ME}}$ as a function of $\bar{\mu}$ as a blue line in Fig. 3(b). The agreement between the exact \bar{T}_c^{ME} and the analytical $\bar{T}_c^{\text{An.sc-ME}}$ is quite good for λ roughly below 0.5. The agreement becomes even better if we extract \bar{T}_c from Eq. (19) by solving it numerically instead of using the approximate analytical result. We show this $\bar{T}_c^{\text{sc-ME}}$ by yellow squares in Fig. 3(b).

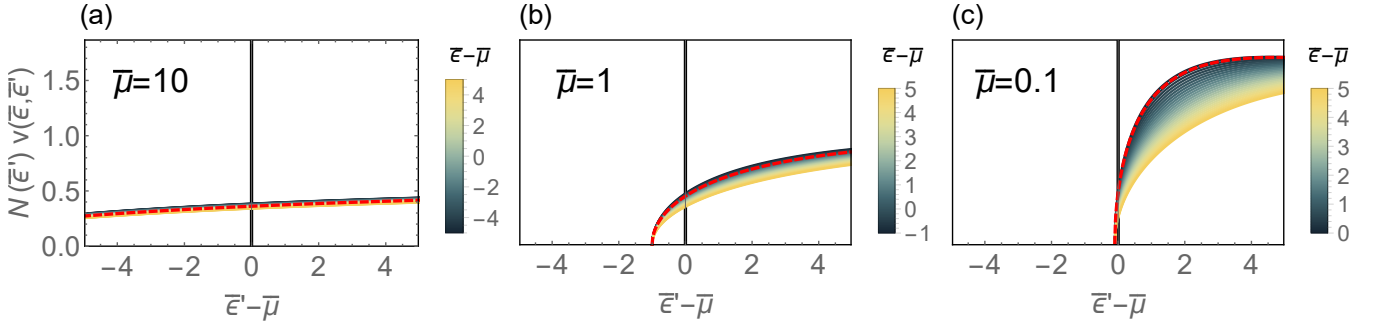


FIG. 2. *The effective dimensionless s-wave coupling constant.* The dimensionless coupling constant is the product of the density of states $N(\bar{\epsilon}') = \sqrt{\bar{\epsilon}'}$ and the s-wave interaction $v(\bar{\epsilon}, \bar{\epsilon}')$, Eq. (14). The product $N(\bar{\epsilon}')v(\bar{\epsilon}, \bar{\epsilon}')$ is plotted for several $\bar{\epsilon}$ in a $\pm 5\omega_L$ energy window of $\bar{\epsilon}'$ around the rescaled chemical potential $\bar{\mu} = \frac{\mu}{\omega_L}$. Panels (a)-(c) are for $\bar{\mu} = 10$, $\bar{\mu} = 1$, and $\bar{\mu} = 0.1$, respectively. The dimensionless coupling acquires a strong energy dependence on $(\bar{\epsilon}, \bar{\epsilon}')$ as $\bar{\mu}$ is reduced. The dashed red line corresponds to $\bar{\epsilon} = \bar{\mu}$. The interception of this lines with $\bar{\epsilon}' - \bar{\mu} = 0$ sets the ME coupling constant λ [Eq.(17)].

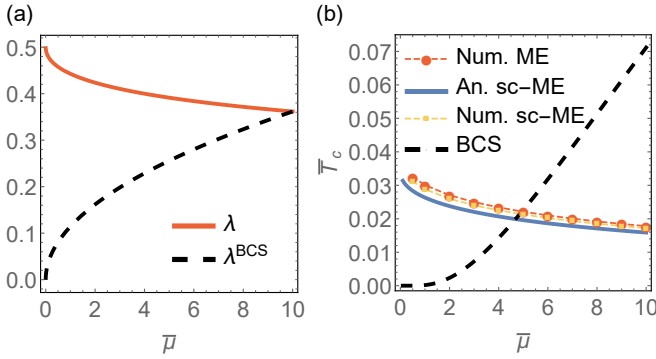


FIG. 3. *The pairing within the ME formalism.* (a) The dimensionless coupling constant. Red line – the dependence of λ from Eq. (17) on $\bar{\mu}$; black dashed line – the BCS coupling $\lambda^{\text{BCS}} = \sqrt{\bar{\mu}v(\bar{\mu} = 10, \bar{\mu} = 10)}$. (b) Critical temperature \bar{T}_c vs $\bar{\mu}$. Red dots – the numerical solution of the ME equation (18); yellow squares – the numerical solution of the ME equation (19) in the small coupling limit; blue line – the analytic solution of the ME equation in the weak coupling limit (Eq. (20)); black dashed line – the canonical BCS expression for T_c , Eq. (30).

For comparison with the full solution of Eqs. (11), (12), and (13) later in the paper, it is instructive to modify the second approximation used to obtain the Eliashberg equations (15) and (16) and keep the integration over $\xi' = \bar{\epsilon}' - \bar{\mu}$ in finite limits, but use the free-fermion Green's functions instead of dressed fermions to compute \bar{Z}_n and $\bar{\chi}_n$. Within this approximation the set (11), (12),

and (13) reduces to

$$Z_n^{(0)} = 1 + \lambda \bar{T} \frac{1}{\bar{\omega}_n} \sum_{n'} u_{n-n'} \bar{\omega}_{n'} \int_{-\bar{\mu}}^{\bar{\Lambda}-\bar{\mu}} d\xi' \frac{1}{\bar{\omega}_{n'}^2 + \xi'^2} \quad (21)$$

$$\bar{\chi}_n^{(0)} = -\lambda \bar{T} \sum_{n'} u_{n-n'} \int_{-\bar{\mu}}^{\bar{\Lambda}-\bar{\mu}} d\xi' \frac{\xi'}{\bar{\omega}_{n'}^2 + \xi'^2} \quad (22)$$

$$\phi_n = \lambda \bar{T} \sum_{n'} u_{n-n'} \int_{-\bar{\mu}}^{\bar{\Lambda}-\bar{\mu}} d\xi' \frac{\phi_{n'}}{[\bar{\omega}_{n'} Z_{n'}^{(0)}]^2 + [\bar{\xi}' + \chi_{n'}^{(0)}]^2} \quad (23)$$

We introduce the superscript (0) to specify that Z_n and $\bar{\chi}_n$ are obtained with free-fermion propagators. The integration over ξ' can again be performed analytically, and the set (21)-(23) reduces to

$$Z_n^{(0)} = 1 + \lambda \frac{\bar{T}}{\bar{\omega}_n} \sum_{n'} u_{n-n'} \zeta_{n'}^{(0)} \quad (24)$$

$$\bar{\chi}_n^{(0)} = -\lambda \bar{T} \sum_{n'} u_{n-n'} \eta_{n'}^{(0)} \quad (25)$$

$$\phi_n = \lambda \bar{T} \sum_{n'} u_{n-n'} \phi_{n'}' \zeta_{n'} \quad (26)$$

where the functions $\zeta_{n'}^{(0)}$, $\eta_{n'}^{(0)}$ and $\zeta_{n'}$ are given by

$$\zeta_{n'}^{(0)} = \frac{1}{\bar{\omega}_{n'}} \left[\arctan \left(\frac{\bar{\Lambda} - \mu}{\bar{\omega}_{n'}} \right) + \arctan \left(\frac{\mu}{\bar{\omega}_{n'}} \right) \right] \quad (27)$$

$$\eta_{n'}^{(0)} = \frac{1}{2} \log \frac{\omega_{n'}^2 + (\bar{\Lambda} - \mu)^2}{\omega_{n'}^2 + \mu^2} \quad (28)$$

$$\zeta_{n'} = \frac{1}{\bar{\omega}_{n'} Z_{n'}} \left[\arctan \left(\frac{\bar{\Lambda} - \mu + \chi_{n'}^{(0)}}{\bar{\omega}_{n'} Z_{n'}^{(0)}} \right) + \arctan \left(\frac{\mu - \chi_{n'}^{(0)}}{\bar{\omega}_{n'} Z_{n'}^{(0)}} \right) \right]. \quad (29)$$

In the infinite bandwidth limit ($\bar{\Lambda} \gg \mu \rightarrow \infty$), $\zeta_{n'}^{(0)} =$

$\frac{\pi}{|\bar{\omega}_{n'}|}$, $\eta_{n'}^{(0)} = 0$, and $\zeta_{n'} = \frac{\pi}{|\bar{\omega}_{n'} Z_{n'}^{(0)}|}$. Then we recover the conventional Eliashberg equations (15)-(16).

We wrap up this Section with a few words on the critical temperature within the "conventional" BCS formalism. In the conventional scenario, an effective electron-phonon interaction v_{eff} is taken to be independent of the chemical potential μ . The density of states of the electron gas in 3 dimensions scales as $\sqrt{\mu}$, hence the dimensionless coupling constant $\lambda^{\text{BCS}} = \sqrt{\mu} v_{\text{eff}}$. We plot λ^{BCS} as a dashed black line in figure 3(a), matching it with our λ at $\bar{\epsilon} = \bar{\epsilon}' = 10$. As $\bar{\mu}$ decreases, λ^{BCS} decreases, hence the critical temperature

$$\bar{T}_c^{\text{BCS}} = 1.13e^{-\frac{1}{\sqrt{\bar{\mu}}v_{\text{eff}}}} \quad (30)$$

gets strongly reduced. We plot this \bar{T}_c^{BCS} as a black dashed line in Fig. 4(b). We see that it is quite different from the actual \bar{T}_c^{ME} , which tends to a constant as $\bar{\mu} \rightarrow 0$.

B. Validity of the ME approximations

We turn now to the analysis of the validity of the two ME approximations as the system moves away from the $\bar{\mu} \gg 1$ regime into the regime where the chemical potential is comparable or even smaller than the characteristic phonon frequency, $\bar{\mu} \ll 1$.

The evolution of the energy dependent coupling constant $N(\bar{\epsilon}')v(\bar{\epsilon}, \bar{\epsilon}')$, which appears in the r.h.s. of Eqs. (11)-(13), is shown in figure 2 for various $\bar{\mu}$. We put $\bar{\epsilon}' - \bar{\mu}$ along the horizontal axis and set it to be in the window $|\bar{\epsilon}' - \bar{\mu}| < 5$. For each value of $\bar{\epsilon}' - \bar{\mu}$ we analyze the variation of $N(\bar{\epsilon}')v(\bar{\epsilon}, \bar{\epsilon}')$ with $\bar{\epsilon} - \bar{\mu}$ by analyzing how much $N(\bar{\epsilon}')v(\bar{\epsilon}, \bar{\epsilon}')$ differs from $N(\bar{\epsilon}')v(\bar{\mu}, \bar{\epsilon}')$, which we present as a dashed red line. The value of $N(\bar{\epsilon}')v(\bar{\mu}, \bar{\epsilon}')$ at $\bar{\epsilon}' = \bar{\mu}$ is the coupling constant λ used in the ME analysis. We see from the figure that $N(\bar{\epsilon}')v(\bar{\epsilon}, \bar{\epsilon}')$ is close to λ at large $\bar{\mu}$, but develops a strong energy dependence when $\bar{\mu}$ becomes small. Consequently, at small $\bar{\mu}$, the energy integration in Eqs. (11)-(13) with and without the restriction to the vicinity of the Fermi level would result in very different normal and anomalous self-energies. We illustrate this in Fig. 4, where we compare the results for the quasiparticle residue $Z_n(\bar{\mu})$, computed in two ways. For definiteness we compare the values of $Z_n^{(0)}(\bar{\mu})$, which, we remind, we compute with free fermions, but integrating over $\bar{\xi}'$ in finite limits. We see from Fig. 4(a) that at large $\bar{\mu}$, $Z_n^{(0)}(\bar{\mu}) - 1$ obtained with an without restriction to the FS are essentially identical. However, for smaller $\bar{\mu}$, $Z_n^{(0)}(\bar{\mu}) - 1$, obtained by keeping the full energy dependence in the coupling constant, substantially increases,

while $Z_n^{(0)}(\bar{\mu}) - 1$ obtained in FS-restricted calculations remains essentially unchanged. We show this in panels (b)-(d) in Fig. 4. The ratio of the two $Z_n^{(0)}(\bar{\mu}) - 1$ reaches 5 for $\bar{\mu} = 0.01$ (see Appendix C for quantitative comparison). Note, however, that the frequency dependence of the actual $Z_n^{(0)}(\bar{\mu}) - 1$ matches well the one of $Z_n^{(0)}(\bar{\mu}) - 1$

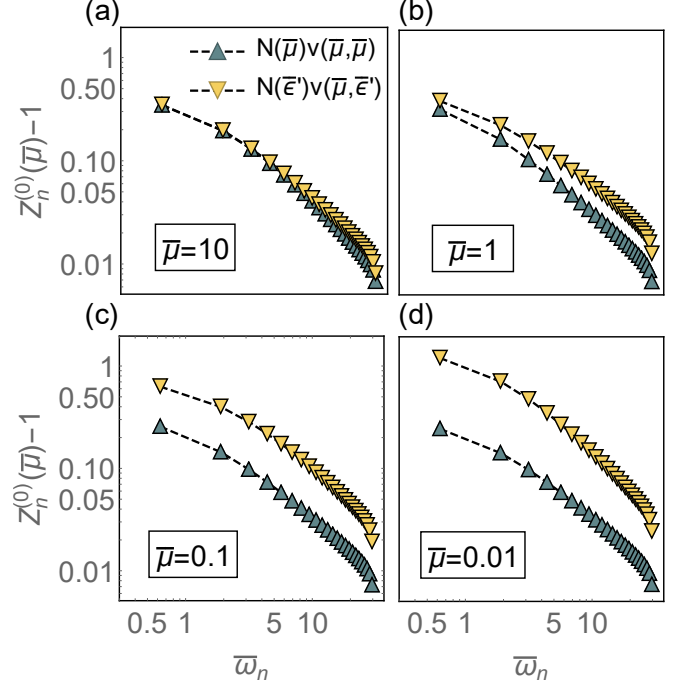


FIG. 4. *The analysis of the restriction to the FS for $Z_n^{(0)}(\bar{\mu})$.* Panels (a)-(d) - the plots of $Z_n^{(0)}(\bar{\mu}) - 1$ vs $\bar{\omega}_n$ in a log-log scale, computed with FS restriction (blue up-triangles) and without it (yellow down-triangles) for different $\bar{\mu}$. (a) $\bar{\mu} = 10$ ($\bar{\kappa}^2 \sim 50$), (b) $\bar{\mu} = 1$ ($\bar{\kappa}^2 \sim 15$), (c) $\bar{\mu} = 0.1$ ($\bar{\kappa}^2 \sim 5$) and (d) $\bar{\mu} = 0.01$ ($\bar{\kappa}^2 \sim 1.5$). In all panels $\bar{T} = 0.2$.

in FS-restricted calculation. The same behavior holds for $Z_n^{(0)}(\bar{\epsilon})$ at other $\bar{\epsilon}$.

We have also studied the additional component of the normal state self-energy, $\chi_n^{(0)}(\bar{\mu})$ [Eq. (22)]. We find that for all values of $\bar{\mu}$, $\chi_n^{(0)}(\bar{\mu})$ is a weakly varying function of the Matsubara frequency, at least for $\bar{\omega}_n < 5$ which give the largest contribution to \bar{T}_c (for details see Appendix C). It is then safe to approximate $\chi_n^{(0)}(\bar{\epsilon})$ by a constant and absorb it into the chemical potential $\bar{\mu}$. We assume that the same holds when we use the full Green's functions instead of the bare ones.

Neglecting $\bar{\chi}_n(\bar{\epsilon})$, we reduce the full set of self-consistent equations for the self-energy to coupled equations for the quasiparticle residue $Z_n(\bar{\epsilon})$ and the pairing vertex $\phi_n(\bar{\epsilon})$:

$$Z_n(\bar{\epsilon}) - 1 = \frac{\bar{T}}{\bar{\omega}_n} \sum_{n'} u_{n-n'} \int_0^{\bar{\Lambda}} d\bar{\epsilon}' \frac{N(\bar{\epsilon}')v(\bar{\epsilon}, \bar{\epsilon}')}{[\bar{\omega}_{n'}Z_{n'}(\bar{\epsilon}')]^2 + [\bar{\epsilon}' - \bar{\mu}]^2} Z_{n'}(\bar{\epsilon}') \quad (31)$$

$$\phi_n(\bar{\epsilon}) = \bar{T} \sum_{n'} u_{n-n'} \int_0^{\bar{\Lambda}} d\bar{\epsilon}' \frac{N(\bar{\epsilon}')v(\bar{\epsilon}, \bar{\epsilon}')}{[\bar{\omega}_{n'}Z_{n'}(\bar{\epsilon}')]^2 + [\bar{\epsilon}' - \bar{\mu}]^2} \phi_{n'}(\bar{\epsilon}'). \quad (32)$$

In Fig. 5 we show $Z_n(\bar{\epsilon})$, obtained by the numerical solution of (31), and compare it with $Z_n^{(0)}(\bar{\epsilon})$. We see that when $\bar{\mu}$ gets smaller, the amplitude of $Z_n(\bar{\epsilon})$ increases at all $\bar{\epsilon}$. This is consistent with the trend we found in Fig. 4(b), and we attribute it to the energy dependence of the coupling constant. In addition, we see from Fig. 5(b)-(d) that $Z_n(\bar{\epsilon})$ acquires significant energy dependence when $\bar{\mu}$ decreases, most notably for the first few Matsubara frequencies. These two features are concomitant by substantial corrections introduced by using the full fermionic propagators. We see from Fig. 5(e)-(h) that the stronger the amplitude and energy dependence of $Z_n(\bar{\epsilon})$, the stronger the difference between the actual $Z_n(\bar{\epsilon})$, which comes out of a self-consistent calculation, and $Z_n^{(0)}(\bar{\epsilon})$ obtained using free fermions.

To summarize: at small $\bar{\mu}$ the contribution from electronic states away from the FS becomes dominant, and consequently, the integration over $\bar{\epsilon}'$ cannot be restricted to the vicinity of the FS. This is the key new feature that invalidates the ME approximation. The modification introduced by self-consistency on $Z_n(\bar{\epsilon})$, on the other hand, is rather modest and not fundamentally relevant. We expect that vertex corrections (the corrections to ladder approximation) will also be at most modest. We now proceed to the calculation of superconducting \bar{T}_c .

C. Critical temperature beyond ME

We solved the set of linearized gap equations (31)-(32) numerically for different $\bar{\mu}$. The results are presented in Fig. 6(a) (red circles). For comparison, we also present the results for \bar{T}_c using $Z_n^{(0)}(\bar{\epsilon})$ instead of the actual $Z_n(\bar{\epsilon})$ (yellow down-triangles) and the analytical expression, $\bar{T}_c^{\text{An.sc-ME}}(\bar{\mu})$, Eq. (20), obtained within the ME formalism at small coupling (black curve). We see that at small $\bar{\mu}$, the actual $\bar{T}_c(\bar{\mu})$ is substantially larger than the approximate small-coupling ME result \bar{T}_c s. To be more specific, the actual $\bar{T}_c(\bar{\mu})$ saturates at around $\bar{T}_c \sim 0.15$ in the limit $\bar{\mu} \rightarrow 0$, while $\bar{T}_c^{\text{An.sc-ME}} \sim 0.034$ in this limit. The difference between the actual \bar{T}_c and the one obtained by evaluating Z with free fermions is about 30% at small $\bar{\mu}$. At large $\bar{\mu}$, $\bar{T}_c(\bar{\mu})$ approaches $\bar{T}_c^{\text{An.sc-ME}}(\bar{\mu})$, as expected.

To understand why \bar{T}_c is quite high at $\bar{\mu} \rightarrow 0$ and what is its dependence on ω_L in this limit, we now obtain an approximate analytical solution of Eqs. (31)-(32). We

first note that, when Z is large, like, e.g., when the system is near a quantum-critical point, the key effect of Z is to cancel the potentially singular $n = n'$ term in the gap equation (such cancellation can be seen in Eq. (18)); other effects of Z are not important. Accordingly, we restrict the frequency summation in the gap equation (32) to $n' \neq n$ and, after that, set $Z_{n'}(\bar{\epsilon}') = 1$. This simplifies the gap equation to

$$\phi_n(\bar{\epsilon}) = \bar{T} \sum_{n' \neq n} u_{n-n'} \int_0^{\bar{\Lambda}} d\bar{\epsilon}' \frac{N(\bar{\epsilon}')v(\bar{\epsilon}, \bar{\epsilon}')}{\bar{\omega}_{n'}^2 + (\bar{\epsilon}' - \bar{\mu})^2} \phi_{n'}(\bar{\epsilon}'). \quad (33)$$

In order to gauge the accuracy of reducing the effect of $Z_n(\bar{\epsilon})$ to the cancellation of $n = n'$ terms in the equation for the pairing vertex, we solved Eq. (33) for \bar{T}_c numerically. We plot the result as green squares in Fig. 6(a) and label it as an "approximate" numerical solution. The evolution of this $\bar{T}_c(\bar{\mu})$ with $\bar{\mu}$ nearly matches that of the actual \bar{T}_c (red circles), while the magnitude is larger by about 35%. This is satisfactory for our purposes, as our goal is to understand the evolution of $\bar{T}_c(\bar{\mu})$ with $\bar{\mu}$ and which combination of parameters sets the scale for $\bar{T}_c(\bar{\mu})$ at small $\bar{\mu}$.

Having verified the validity of Eq. (33), we continue with the analytic analysis. We conjecture that in the $\bar{\mu} = 0$ limit, this equation can be simplified further. Based again on potential analogy with the pairing problem near a Quantum-Critical point, we assume and then verify that to extract $\bar{T}_c^{\text{an}}(\bar{\mu} = 0)$ from (33) one can restrict the sum to the first few Matsubara frequencies, more specifically to $\bar{\omega}_n = \pm\pi\bar{T}$. This approximation eliminates the frequency summation in (33) and reduces it to a 1D integral equation for $\phi_0(\bar{\epsilon}) = \phi_{-1}(\bar{\epsilon})$:

$$\tilde{\phi}_0(\bar{p}) = \frac{2\sqrt{\bar{\rho}}\bar{T}/\pi}{1 + (2\pi\bar{T})^2} \int_0^\infty d\bar{p}' \frac{\log\left(\frac{\bar{p} + \bar{p}'}{|\bar{p} - \bar{p}'|}\right)}{(\pi\bar{T})^2 + \bar{p}'^4} \tilde{\phi}_0(\bar{p}'). \quad (34)$$

Here we switched to the radial momentum variable $\bar{p}' = \sqrt{\bar{\epsilon}'}$, and introduced the rescaled variable $\tilde{\phi}_0(\bar{p}) = \bar{p}\phi_0(\bar{p})$. Solving this equation (see Appendix D for details), we obtain the following relation for \bar{T}_c ,

$$\sqrt{\pi\bar{T}_c^{\text{an}}} [1 + 4(\pi\bar{T}_c^{\text{an}})^2] = \frac{8}{(5 - \sqrt{10})\pi^2} \sqrt{\bar{\rho}}, \quad (35)$$

where, we remind $\bar{\rho} = \frac{\text{Ry}}{\omega_L}$. Because the Rydberg energy (Ry = 13.6 eV) is in general much larger than the characteristic phonon frequency ω_L , i.e. $\bar{\rho} \gg 1$, Eq. (35) can

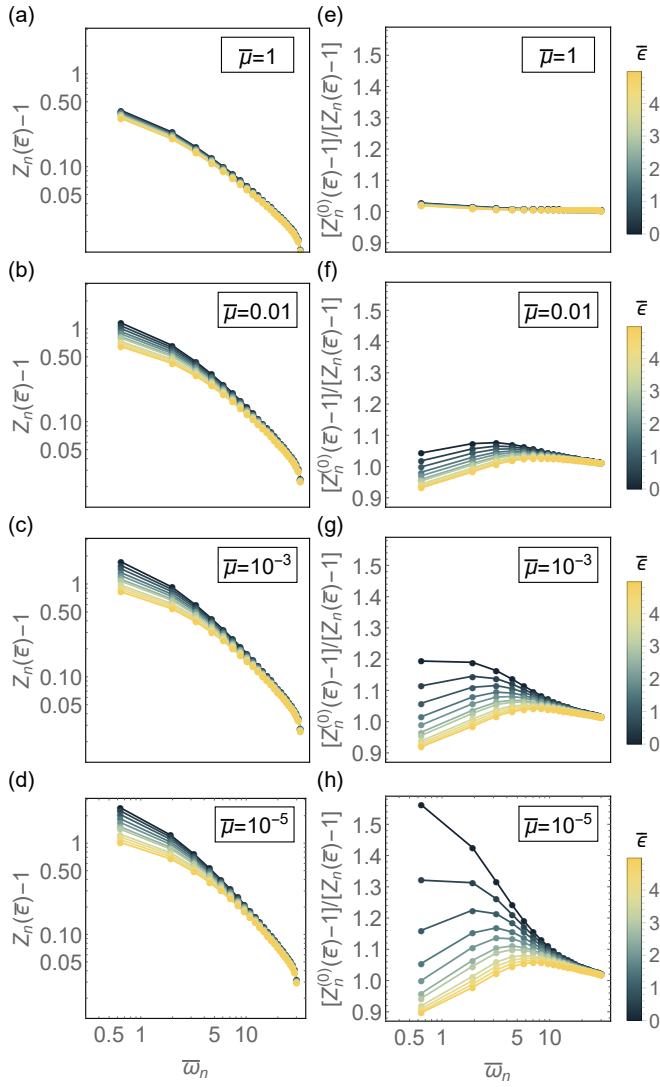


FIG. 5. *The role of self-consistency for fermionic $Z_n(\bar{\epsilon})$.* Panels (a)-(d) – $Z_n(\bar{\epsilon}) - 1$ from Eq. (31) vs $\bar{\omega}_n$ in a log-log scale, at various $\bar{\mu}$, indicated in legends. (e)-(h) The ratio between $Z_n^{(0)}(\bar{\epsilon}) - 1$ computed with free fermions and the self-consistent expression $Z_n(\bar{\epsilon}) - 1$ for those same $\bar{\mu}$.

be solved by expanding in $1/\bar{\rho}$. We then obtain

$$\bar{T}_c^{\text{an}} \simeq \frac{1}{\pi} \left[\frac{2}{\pi^2(5 - \sqrt{10})} \right]^{\frac{2}{5}} \bar{\rho}^{\frac{1}{5}} \longrightarrow T_c^{\text{an}} \simeq 0.13\omega_L \left(\frac{\text{Ry}}{\omega_L} \right)^{\frac{1}{5}} \quad (36)$$

We see that, in the actual dimension-full units, T_c^{an} contains ω_L as the overall factor, but also contains an enhancement factor Ry/ω_L with the non-trivial exponent $1/5$.

We verified this functional form by plotting in Fig. 6(b) various numerical \bar{T}_c 's from Fig. 6(a) as functions of ω_L . We see that the actual \bar{T}_c , and \bar{T}_c obtained in approximate numerical calculations follow $\omega_L^{-1/5}$ behavior quite well. As an independent check, we fitted the actual \bar{T}_c by $\omega_L^{-\eta}$ and obtained $\eta \approx 1/6$, which is quite close to the

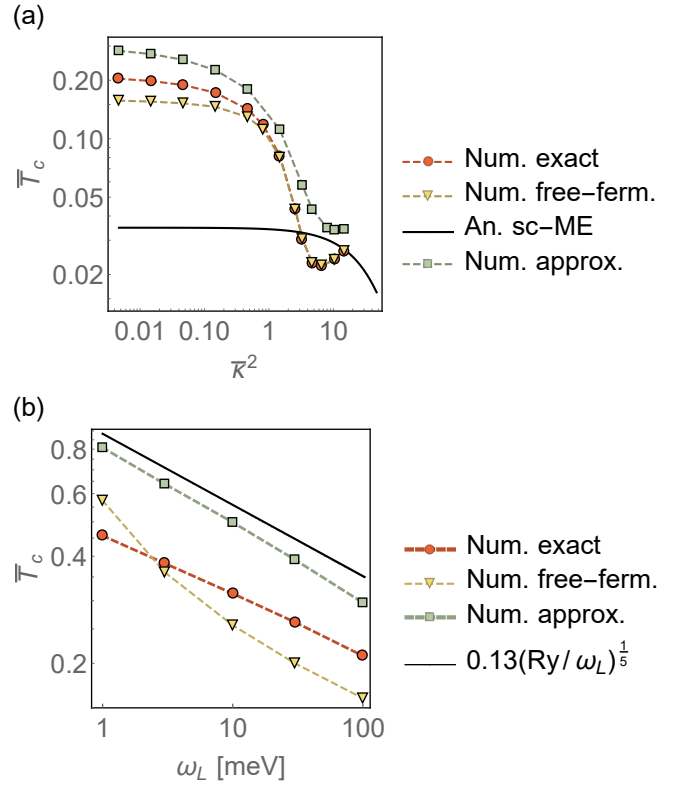


FIG. 6. *Superconducting $\bar{T}_c = \frac{T_c}{\omega_L}$.* (a) \bar{T}_c versus the rescaled screening $\bar{\kappa}^2 = \frac{\kappa^2/2m}{\omega_L} = \frac{4}{\pi} \sqrt{\bar{\mu}\bar{\rho}}$. Red circles – the numerical solution of Eq. (32) with the actual $Z_n(\bar{\epsilon})$ given by Eq. (31); yellow triangles – the numerical solution of Eq. (32) with the approximate (non-self-consistent) $Z_n^{(0)}(\bar{\epsilon})$, computed with free fermions; black line – the ME expression at small coupling, Eq. (20); green squares – the numerical solution of the approximate gap equation (33). In all cases we set $\omega_L = 100$ meV. (b) Numerical solutions in the $\bar{\mu} = 0$ limit as a function of phonon frequency ω_L for three computational procedures described for panel (a) (specified in the legend). The black line is the analytical expression \bar{T}_c^{an} [Eq. (36)].

analytical result $\eta = \frac{1}{5}$.

IV. SUMMARY

Phonon-mediated superconductivity has been extensively studied within the Migdal-Eliashberg framework, which is suitable for conventional metals with $\mu \gg \omega_L$. In this work, we analyzed pairing in the opposite regime of low carrier density, where $\mu \ll \omega_L$, which is believed to be relevant to several bulk systems, most notably SrTiO₃ and Bi. By considering the attractive part of the Coulomb-screened electron-phonon interaction, both the frequency and momentum dependencies of the pairing interaction were included. We showed that the contribution to the mass renormalization function and pairing vertex are dominated by electronic states away from the FS. This result is in stark contrast to the

more standard regime $\mu \gg \omega_L$, where these processes can be safely neglected and the computation of the fermionic self-energy can be confined to the vicinity of the FS. More specifically, we solved the momentum- and frequency-dependent gap equations to obtain the pairing instability temperature T_c as a function of μ/ω_L . We found, both numerically and analytically, a substantial increase of the critical temperature T_c in the limit $\mu \rightarrow 0$. In fact, the value of T_c not only remains finite in this limit, but exceeds the characteristic phonon frequency ω_L . We obtained the analytical result $T_c \propto \omega_L \left(\frac{\text{Ry}}{\omega_L}\right)^\eta$, with $\eta = \frac{1}{5}$, for $\mu \rightarrow 0$, which agrees well with our numerical results for $T_c(\omega_L)$. Future investigations that include also the repulsive part of the Coulomb-screened electron-phonon interaction are desirable, particularly since in the $\mu \ll \omega_L$ limit there is a very narrow window for the renormalization of the Coulomb repulsion into a reduced effective pseudopotential.

ACKNOWLEDGMENTS

We thank K. Behnia, G. Lonzarich, D.L. Maslov and A. Aperis for fruitful discussions. This work was supported by the U. S. Department of Energy through the University of Minnesota Center for Quantum Materials,

under Award No. DE-SC-0016371.

Appendix A: Effective interaction and the $\omega_q \rightarrow \omega_L$ approximation

The difference between the renormalized phonon frequency ω_q and the bare frequency ω_L has not been included in the electron-phonon interaction Eq. (4). Here we show that the renormalization of ω_L can be neglected for the superconducting channel within the leading logarithmic approximation. The term that has not been included in Eq. (4) is

$$f_n(q) = -\frac{\bar{\Omega}_n^2}{1 + \bar{\Omega}_n^2} \frac{\kappa^2}{q^2 (1 + \bar{\Omega}_n^2) + \kappa^2 \bar{\Omega}_n^2}. \quad (\text{A1})$$

We follow the notation in the main text, with an overbar denoting a rescaled variable with respect to the bare phonon frequency, $\bar{\Omega}_n = \frac{\Omega_n}{\omega_L}$. After the angular integration is performed, the s-wave component of the electron-phonon term when ω_q is included is

$$V_n^{\text{el-ph}}(\bar{p}, \bar{p}') = \frac{1}{1 + \bar{\Omega}_n^2} [v(\bar{p}, \bar{p}') + \mathcal{F}_n(\bar{p}, \bar{p}')], \quad (\text{A2})$$

where $v(\bar{p}, \bar{p}')$ is the radial momentum dependent term that has been included in our model [Eq. (14)], and $\mathcal{F}_n(\bar{p}, \bar{p}')$ is the additional contribution coming from the renormalized frequency, the $f_n(q)$ term [Eq. (A1)]:

$$\mathcal{F}_n(\bar{p}, \bar{p}') = -\bar{\Omega}_n^2 \frac{\sqrt{\bar{p}}}{2\pi\bar{p}\bar{p}'} \log \left[1 + \frac{4\bar{\kappa}^2 \bar{p}\bar{p}'}{[(\bar{p} - \bar{p}')^2 (1 + \bar{\Omega}_n^2) + \bar{\Omega}_n^2 \bar{\kappa}^2] [(\bar{p} + \bar{p}')^2 + \bar{\kappa}^2]} \right]. \quad (\text{A3})$$

We now insert the electron-phonon interaction (A2) in the fermionic self-energy equations (11)-(13) and apply the ME approximations described in the main text. By expanding for small coupling to first order in λ , $Z_n = 1 + \lambda + \mathcal{O}(\lambda^2)$ and we get for the pairing vertex the following

equation,

$$\phi_n = \lambda^* \sum_{n'} \chi_{n-n'} \frac{\pi \bar{T}}{|\bar{\omega}_{n'}|} \phi_{n'} \quad (\text{A4})$$

instead of Eq. (19), where the propagator $\chi_{n-n'}$ has acquired an additional term,

$$\chi_{n-n'} = \frac{1}{1 + |\bar{\omega}_n - \bar{\omega}_{n'}|^2} - \frac{|\bar{\omega}_n - \bar{\omega}_{n'}|^2}{1 + |\bar{\omega}_n - \bar{\omega}_{n'}|^2} \frac{\log \left(1 + \frac{1}{|\bar{\omega}_{n'}|^2} \frac{1}{1+\alpha} \right)}{\log \left(1 + \frac{1}{\alpha} \right)} \quad (\text{A5})$$

with $\alpha = \frac{1}{\pi} \sqrt{\frac{\text{Ry}}{\mu}}$. In order to get an estimate of the contribution of this additional term in the propagator to T_c , we neglect the $\bar{\omega}_n$ dependence in $\chi_{n-n'}$, and the gap

equation is further simplified

$$1 = \lambda^* \sum_{n'} \frac{1}{1 + |\bar{\omega}_{n'}|^2} \left[1 - |\bar{\omega}_{n'}|^2 \frac{\log \left(1 + \frac{1}{|\bar{\omega}_{n'}|^2} \frac{1}{1+\alpha} \right)}{\log \left(1 + \frac{1}{\alpha} \right)} \right] \frac{\pi \bar{T}}{|\bar{\omega}_{n'}|} \quad (\text{A6})$$

$$\simeq -\lambda^* \log(\pi \bar{T}) + \mathcal{O}(\lambda^*).$$

As seen, the leading logarithmic contribution is given by the first term (which we have included in our model), and the contribution from the second term (coming from the renormalization of ω_L by the electronic screening) is linear in λ^* and without a logarithm. We thus neglect this contribution and use the effective interaction (4).

Appendix B: The derivation of the gap equations

In this section we present the details of the derivation of the fermionic self-energy equations (11)-(13) for the

effective electron-phonon interaction,

$$V_n^{\text{e-ph}}(q) = -\frac{4\pi e^2}{q^2 + \kappa^2} \frac{\omega_L^2}{\Omega_n^2 + \omega_L^2}. \quad (\text{B1})$$

The various components of the equations are in terms of the dimension-full variables,

$$\frac{1}{\omega_L} \int_0^{\sqrt{2m\Lambda}} \frac{dk'k'^2}{2\pi} \frac{1}{2\pi} \int_{-1}^1 dx P_{l=0}(x) \frac{4\pi e^2}{k^2 + k'^2 - 2kk'x + \kappa^2} = \int_0^{\bar{\Lambda}} d\bar{\epsilon}' N(\bar{\epsilon}') v(\bar{\epsilon}, \bar{\epsilon}') \quad (\text{B2})$$

$$\frac{\omega_L^2}{\omega_L} \frac{T}{[\bar{\omega}_{n'} Z_{n'}(k')]^2 + [\epsilon' - \mu + \chi_{n'}(k')]^2} = \frac{\bar{T}}{[\bar{\omega}_{n'} Z_{n'}(\bar{\epsilon}')]^2 + [\bar{\epsilon}' - \bar{\mu} + \bar{\chi}_{n'}(\bar{\epsilon}')]^2}, \quad (\text{B3})$$

with the first Legendre polynomial $P_{l=0}(x) = 1$ for the isotropic s-wave component of the interaction.

Appendix C: FS restriction of $Z_n^{(0)}(\bar{\mu})$ and $\bar{\chi}_n^{(0)}(\bar{\mu})$

Figure 7 shows the normal state components of the self-energy $Z_n^{(0)}(\bar{\mu}) - 1$ and $\bar{\chi}_n^{(0)}(\bar{\mu})$, which were discussed in Section III B. They are computed in two different ways: (i) by keeping the energy dependence of the coupling constant $N(\bar{\epsilon}')v(\bar{\epsilon}, \bar{\epsilon}')$ and (ii) restricting the calculation to the FS vicinity $N(\bar{\mu})v(\bar{\mu}, \bar{\mu})$. Panels (a)-(d) illustrate the quantitative comparison of the mass renormalization computed with and without the FS restriction (blue and yellow data, respectively). The FS restricted function has been renormalized by the number specified in each panel to match the $n = 0$ Matsubara frequency of the non-FS restricted function. For high $\bar{\mu}$, $Z_n^{(0)}(\bar{\mu}) - 1$ computed with and without the FS restriction are almost identical. As the chemical potential is reduced, the non-FS restricted computation (yellow data) results in higher mass renormalization. On the contrary, the FS restricted result (blue data) stays nearly unchanged and for a quantitative comparison, we show this data renormalized by the number specified in each panel [Figs. 7(b)-(d)]. It reaches almost a factor of 5 difference for $\bar{\mu} = 0.01$, which highlights the dominant contribution of the states far from the FS in the $\bar{\mu} \ll 1$ regime.

The energy shift function $-\bar{\chi}_n^{(0)}(\bar{\mu})$ is also shown for the same parameters in Fig. 7(e)-(h). As seen, the electronic processes away from the FS dominate this self-energy component as well in the dilute $\bar{\mu} \ll 1$ limit. The FS-restricted results have been renormalized by the same number as in panels (a)-(d) for clarity. In all cases $\bar{\chi}_n^{(0)}(\bar{\mu})$

is a weakly varying function of $\bar{\omega}_n$ for $\bar{\omega}_n < 5$.

Appendix D: Derivation of the \bar{T}_c expression at $\bar{\mu} = 0$

We give below the detailed solution of the gap equation (34),

$$\phi(\bar{p}) = \frac{2\sqrt{\bar{\rho}\bar{T}}/\pi}{1 + (2\pi\bar{T})^2} \int_0^\infty d\bar{p}' \frac{\log\left(\frac{\bar{p} + \bar{p}'}{|\bar{p} - \bar{p}'|}\right)}{(\pi\bar{T})'^2 + \bar{p}'^4} \phi(\bar{p}') \quad (\text{D1})$$

to obtain the relation for \bar{T}_c given by Eq. (35). By making the change of variables $x = \frac{\bar{p}'}{\sqrt{\pi\bar{T}}}$ and $y = \frac{\bar{p}}{\sqrt{\pi\bar{T}}}$ the equation becomes

$$\phi(y) = C \int_0^\infty dx \frac{1}{1 + x^4} \log\left(\frac{y + x}{|y - x|}\right) \phi(x) \quad (\text{D2})$$

where

$$C = \frac{2\sqrt{\bar{\rho}}}{\pi^2} \frac{1}{\sqrt{\pi\bar{T}} [1 + (2\pi\bar{T})^2]} \quad (\text{D3})$$

and we have taken $\sqrt{\Lambda/\pi\bar{T}} \rightarrow \infty$. We then consider the two limits $x \gg y$ and $x \ll y$ and approximate the logarithm and gap function accordingly,

$$\log\left(\frac{1 + z}{|1 - z|}\right) = \begin{cases} 2/z & \text{if } z \gg 1 \\ 2z & \text{if } z \ll 1 \end{cases} \quad (\text{D4})$$

with $z = \frac{x}{y}$. We then look for gap function solutions of the form

$$\phi(z) = \begin{cases} A/z & \text{if } z \gg 1 \\ Bz & \text{if } z \ll 1 \end{cases} \quad (\text{D5})$$

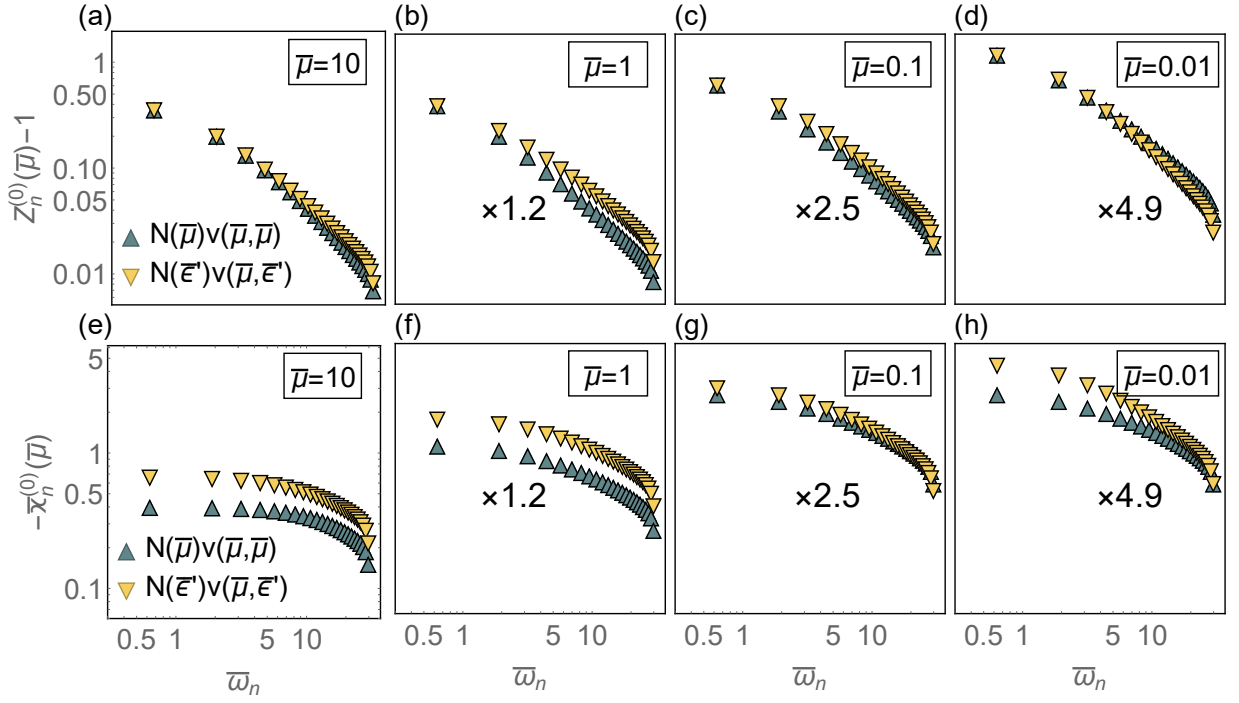


FIG. 7. Mass renormalization $Z_n^{(0)}(\bar{\mu}) - 1$ vs $\bar{\omega}_n$ in a log-log scale for (a) $\bar{\mu} = 10$, (b) $\bar{\mu} = 1$, (c) $\bar{\mu} = 0.1$, and (d) $\bar{\mu} = 0.01$ computed with FS restriction (blue up-triangles) and keeping the full energy dependence (yellow down-triangles). The blue data has been renormalized by the number specified in each panel to match the first Matsubara frequency of the yellow data. Panels (e)-(h) – the same plots for the energy-shift function $-\bar{\chi}_n^{(0)}(\bar{\mu})$. In all panels $\bar{T} = 0.2$.

and the get the following set of coupled equations,

$$\begin{cases} \frac{A}{y} = C \left(\int_0^1 dx \frac{2x}{y} Bx + \int_1^\infty dx \frac{1}{x^4} \frac{2x}{y} \frac{A}{x} \right) \\ By = C \left(\int_0^1 dx \frac{2y}{x} Bx + \int_1^\infty dx \frac{1}{x^4} \frac{2y}{x} \frac{A}{x} \right). \end{cases} \quad (\text{D6})$$

Solving these equations we get the condition for C

$$\begin{vmatrix} 1 - \frac{2}{3}C & \frac{2}{3}C \\ \frac{2}{3}C & 2C - 1 \end{vmatrix} = 0, \quad (\text{D7})$$

which gives $C = \frac{1}{4} (5 - \sqrt{10})$ at \bar{T}_c . Finally, by equating this coefficient to the initial temperature dependent expression in Eq. (D3) we recover Eq. (35) for \bar{T}_c at $\bar{\mu} = 0$,

$$\frac{2\sqrt{\bar{\rho}}}{\pi^2} \frac{1}{\sqrt{\pi\bar{T}_c} [1 + (2\pi\bar{T}_c)^2]} = \frac{1}{4} (5 - \sqrt{10}). \quad (\text{D8})$$

-
- [1] F. Wang and D.-H. Lee, *Science* **332**, 200 (2011); P. J. Hirschfeld, M. M. Korshunov, and I. I. Mazin, *Reports on Progress in Physics* **74**, 124508 (2011); R. Fernandes and A. Chubukov, *Rep. Prog. Phys.* **80**, 014503 (2017); A. Chubukov, *Springer Series in Materials Science* **211**, 255 (2015).
- [2] L. V. Gurevich, A. Larkin, and Y. A. Firsov, *Sov. Phys. Sol. State* **4**, 185 (1962).
- [3] J. F. Schooley, W. R. Hosler, and M. L. Cohen, *Phys. Rev. Lett.* **12**, 474 (1964).
- [4] J. F. Schooley, W. R. Hosler, E. Ambler, J. H. Becker, M. L. Cohen, and C. S. Koonce, *Phys. Rev. Lett.* **14**, 305 (1965).
- [5] I. A. Chernik and S. N. Lykov, *Sov. Phys. Solid State* **23**, 817 (1981).
- [6] Y. Takada, *JPSJ* **49**, 1267 (1980).
- [7] M. Ikeda, A. Ogasawara, and M. Sugihara, *Physics Letters A* **170**, 319 (1992).
- [8] C. Grimaldi, L. Pietronero, and S. Strässler, *Phys. Rev. Lett.* **75**, 1158 (1995).
- [9] X. Lin, G. Bridoux, A. Gourgout, G. Seyfarth, S. Krämer, M. Nardone, B. Fauqué, and K. Behnia, *Phys. Rev. Lett.* **112**, 207002 (2014).
- [10] Y. Nakajima, R. Hu, K. Kirshenbaum, A. Hughes, P. Syers, X. Wang, K. Wang, R. Wang, S. R. Saha, D. Pratt, J. W. Lynn, and J. Paglione, *Sci. Adv.* **1**, e1500242 (2015).
- [11] O. Prakash, A. Kumar, A. Thamizhavel, and S. Ramakrishnan, *Science* **355**, 52 (2017).
- [12] J. M. Edge, Y. Kedem, U. Aschauer, N. A. Spaldin, and A. V. Balatsky, *Phys. Rev. Lett.* **115**, 247002 (2015).
- [13] J. Ruhman and P. A. Lee, *Phys. Rev. B* **94**, 224515 (2016).
- [14] L. P. Gor'kov, *Phys. Rev. B* **93**, 054517 (2016).
- [15] L. P. Gorkov, *J Supercond Nov Magn* **30**, 845 (2017).

- [16] J. Ruhman and P. A. Lee, Phys. Rev. B **96**, 235107 (2017).
- [17] T. V. Trevisan, M. Schütt, and R. M. Fernandes, Phys. Rev. Lett. **121**, 127002 (2018).
- [18] L. Savary, J. Ruhman, J. W. F. Venderbos, L. Fu, and P. A. Lee, Phys. Rev. B **96**, 214514 (2017).
- [19] S. E. Rowley, C. Enderlein, J. Ferreira de Oliveira, D. A. Tompsett, E. Baggio Saitovitch, S. S. Saxena, and G. G. Lonzarich, arXiv preprint arXiv:1801.08121 (2018).
- [20] M. Coak, C. Haines, C. Liu, S. Rowley, G. G. Lonzarich, and S. S. Saxena, arXiv preprint arXiv:1808.02428 (2018).
- [21] P. Wölfle and A. V. Balatsky, Phys. Rev. B **98**, 104505 (2018).
- [22] M. Sadoyskii, arXiv preprint arXiv:1809.02531 (2018).
- [23] M. Sadoyskii, arXiv preprint arXiv:1811.10184 (2018).
- [24] G. M. Eliashberg, JETP **11**, 696 (1960).
- [25] A. Migdal, Sov. Phys. JETP **7**, 996 (1958).
- [26] D. Scalapino, New York **1** (1969).
- [27] J. P. Carbotte, Rev. Mod. Phys. **62**, 1027 (1990).
- [28] F. Marsiglio and J. P. Carbotte, “Superconductivity: Volume 1: Conventional and unconventional superconductors,” (Springer Science & Business Media, 2008) Chap. Electron-Phonon Superconductivity, pp. 73–162.
- [29] R. Haslinger and A. V. Chubukov, Phys. Rev. B **68**, 214508 (2003).
- [30] P. Morel and P. Anderson, Phys. Rev. **125**, 1263 (1962).
- [31] D. J. Scalapino, J. R. Schrieffer, and J. W. Wilkins, Phys. Rev. **148**, 263 (1966).
- [32] W. McMillan, Phys. Rev. **167**, 331 (1968); N. Bogolubov, A New Method in the Theory of Superconductivity, Consultant Bureau, New York (1959).
- [33] P. Coleman, *Introduction to many-body physics* (Cambridge University Press, 2015).
- [34] P. Monthoux, A. V. Balatsky, and D. Pines, Phys. Rev. Lett. **67**, 3448 (1991).
- [35] D. J. Scalapino, Rev. Mod. Phys. **84**, 1383 (2012).
- [36] A. Abanov, A. Chubukov, and J. Schmalian, Advances in Physics **52**, 119 (2003).
- [37] I. Mazin, D. J. Singh, M. Johannes, and M.-H. Du, Phys. Rev. Lett. **101**, 057003 (2008).
- [38] K. Kuroki, S. Onari, R. Arita, H. Usui, Y. Tanaka, H. Kontani, and H. Aoki, Phys. Rev. Lett. **101**, 087004 (2008).
- [39] A. V. Chubukov, D. V. Efremov, and I. Eremin, Phys. Rev. B **78**, 134512 (2008).
- [40] S. Maiti and A. Chubukov, Proceedings of the XVII Training Course in the physics of Strongly Correlated Systems (2014).
- [41] M. L. Cohen, Phys. Rev. **134**, A511 (1964).
- [42] C. Castellani, C. Di Castro, and M. Grilli, Phys. Rev. Lett. **75**, 4650 (1995).
- [43] A. A. Golubov and I. I. Mazin, Phys. Rev. B **55**, 15146 (1997).
- [44] J. Bardeen and D. Pines, Phys. Rev. **99**, 1140 (1955).
- [45] G. D. Mahan, *Many-particle physics* (Springer Science & Business Media, 2000).
- [46] J. R. Engelbrecht, M. Randeria, and C. A. R. Sáde Melo, Phys. Rev. B **55**, 15153 (1997).
- [47] C. A. R. Sá de Melo, M. Randeria, and J. R. Engelbrecht, Phys. Rev. Lett. **71**, 3202 (1993).
- [48] A. V. Chubukov, I. Eremin, and D. V. Efremov, Phys. Rev. B **93**, 174516 (2016).
- [49] A. Aperis and P. M. Oppeneer, Phys. Rev. B **97**, 060501 (2018).
- [50] F. Schrodi, A. Aperis, and P. M. Oppeneer, Phys. Rev. B **98**, 094509 (2018).
- [51] A. E. Karakozov, E. G. Maksimov, and S. A. Mashkov, Sov. Phys. JETP **41**, 971 (1975).
- [52] O. V. Dolgov, I. I. Mazin, A. A. Golubov, S. Y. Savrasov, and E. G. Maksimov, Phys. Rev. Lett. **95**, 257003 (2005).
- [53] Y. Wang and A. Chubukov, Phys. Rev. B **88**, 024516 (2013).
- [54] F. Marsiglio, Phys. Rev. B **98**, 024523 (2018).